

High-resolution X-ray diffraction beamline at the LNLS for the study of charge, orbital and magnetic structures

C. Giles,^{a,b*} F. Yokaichiya,^a S. W. Kycia,^b
 L. C. Sampaio,^c D. C. Ardiles-Saravia,^b
 M. K. K. Franco^a and R. T. Neuenschwander^b

^aInstituto de Física, Universidade Estadual de Campinas, SP, Brazil, ^bLaboratório Nacional de Luz Síncrotron, Campinas, SP, Brazil, and ^cCBPF, Rio de Janeiro, RJ, Brazil.
 E-mail: giles@ifi.unicamp.br

A high-resolution X-ray diffraction beamline at the Brazilian Synchrotron Light Laboratory (LNLS) has been commissioned for the study of crystalline magnetic materials. The beamline optics is based on a Rh-coated vertical-focusing X-ray mirror and a sagittal-focusing double-crystal monochromator. The primary instrument is a six-circle diffractometer equipped with energy and polarization analysers and a closed-cycle He cryostat. The beamline source is a bending magnet of the 1.37 GeV storage ring of the LNLS, delivering approximately 4×10^{10} photons s^{-1} at 8 keV at the sample position. Resonant and non-resonant scattering are the main techniques used to study charge, orbital and magnetic structures. Examples of magnetic scattering in Ho and NiO single crystals, as well as orbital ordering in manganites thin films, are presented.

Keywords: X-ray magnetic scattering; beamline optics; instrumentation.

1. Introduction

High-resolution X-ray scattering at synchrotron sources has become an important tool for the study of charge, orbital and magnetic structures in condensed-matter physics. The successful operation of the Brazilian Synchrotron Light Laboratory (LNLS) in Campinas, Brazil, has opened the way to the use of this unique technique in Latin America. The challenge of building an X-ray diffraction beamline at the LNLS capable of performing magnetic scattering and orbital-ordering measurements is described in this paper. The installation of a high-resolution diffraction beamline that allows experiments of resonant and non-resonant magnetic scattering with polarization analysis at the LNLS is certainly a contribution to the expansion of this technique for the local magnetic community.

In this paper we describe the XRD2 beamline located at the D10A bending-magnet port at the LNLS. The beamline optics, the experimental end-station, as well as some commissioning results, are reported. The source characteristics, beamline optics, experimental end-station and sample environment are then described. Finally, first measurements of magnetic scattering in typical samples and orbital-ordering measurements in thin films are outlined.

2. LNLS source and beamline optics

2.1. Synchrotron light source

The LNLS synchrotron light source is composed of a 1.37 GeV electron storage ring, with a 500 MeV booster synchrotron and a 120 MeV linear accelerator. Forthcoming upgrades to the storage-ring RF cavity and changes to the dipole vacuum chambers in 2004 will allow the beam current in the storage ring to increase from the

Table 1

Beamline and storage-ring parameters of bending-magnet beamlines using X-ray magnetic scattering.

The electron energy (E), the nominal current (I) and the maximum horizontal and vertical angular acceptance of the corresponding beamline optics (mradH and mradV) described here were used in the calculations of the spectral flux shown in Fig. 1. ESRF: European Synchrotron Radiation Facility, France. APS: Advanced Photon Source, USA. NSLS: National Synchrotron Light Source, USA. ALS: Advanced Light Source, USA. LNLS: Brazilian Synchrotron Light Laboratory, Brazil.

Beamline	E (GeV)	I (mA)	mradH	mradV
XMas ESRF	6.0	200	3.1	0.2
IBM APS	7.0	200	3.7	0.1
X22C NSLS	2.58	250	2.1	0.25
9.3.2 ALS	1.9-1.5	400	2.0	0.2
XRD2 LNLS	1.37	100	5.0	0.6

current 250 mA to a projected current of 400 mA. As with all beamlines at the LNLS, the XRD2 beamline is installed at a 1.67 T bending-magnet port. The flux produced by the bending-magnet source with a current of 100 mA can be compared with similar bending-magnet-based beamlines devoted to magnetic scattering (Fig. 1). At 8 keV the monochromatic intensity at the sample of the XRD2 beamline is an order of magnitude smaller than at the X22C beamline at NSLS (Brookhaven National Laboratory, USA). The expected increase in the stored current at the LNLS will decrease this difference by a factor of four, allowing this beamline to be competitive.

2.2. Beamline optics

The beamline optics is composed of two main optical elements. The first is a vertically focusing cylindrically bent Rh-coated ultra-low-expansion X-ray mirror. The total heat load on the mirror located after a water-cooled Be window is of the order of 2 W, leading to a reduced heat-load density and no need for a cooling system at the mirror. The mirror was purchased from Zeiss of Germany and the bending mechanism and vacuum chamber were designed and built at

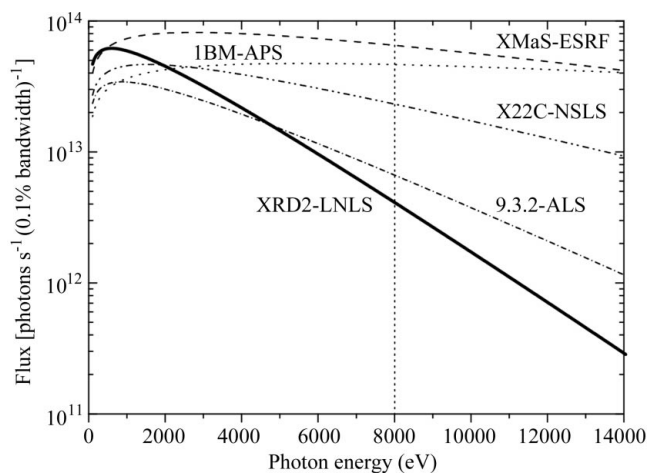


Figure 1

Photon flux of the XRD2 beamline at LNLS compared with other bending-magnet beamlines performing X-ray magnetic scattering. Calculations take into account nominal values for energy and current of the respective storage ring as well as available focusing optics of each beamline and are outlined in Table 1. The LNLS photon flux considers a 5 mrad horizontal acceptance from sagittal focusing and 0.6 mrad vertical acceptance from a meridional-focusing mirror.

the LNLS (Neuenschwander, 2002). The double-bounce monochromator consists of a flat water-cooled first crystal and a dynamically bent sagittal crystal. The crystals used are Si(111), prepared at the LNLS. The monochromator is located in a one-to-one configuration regarding the source-to-monochromator and monochromator-to-sample distances, allowing an optimized configuration of the beam size at the sample and horizontal angular acceptance. Since the beamline will typically be working in an energy range below 12 keV, the efficiency of the monochromator is high for the entire horizontal angular range accepted (Sparks *et al.*, 1982). The sagittal-focusing crystal is triangularly shaped and is clamped at its base; its apex rests on a polished fixed point allowing a cylindrical curvature to be obtained by applying a torque at the crystal base. The tilting, angular optimizations and the bend radius are adjusted remotely by computer-controlled stepping motors. Both crystals are fixed in a rotation goniometer controlled by a translation stage outside the

vacuum chamber connected by a 100 μm thin steel strip (Correa *et al.*, 1992). A single 0.5 μm step of the translation stage results in an angular step and resolution of 5 μrad . The double-crystal monochromator can operate in a constant offset mode by varying the vertical position of the second crystal by means of a precise linear-translation stage. The overall layout of the main optical elements of the beamline is shown in Fig. 2.

Under these conditions the typical beam size at the sample position is of the order of 0.5 mm \times 0.5 mm. The energy range covered by the beamline optics is between 3 keV and 15 keV. The lower limit is imposed by the absorption losses by Be windows and the upper limit is fixed by the source and cut-off energy of the X-ray mirror. Additional beamline components, *i.e.* motorized slits, X-ray beam-position monitors, adjustable filters, vacuum flight paths and ion chambers, are assembled along the beamline and were designed and built at the LNLS.

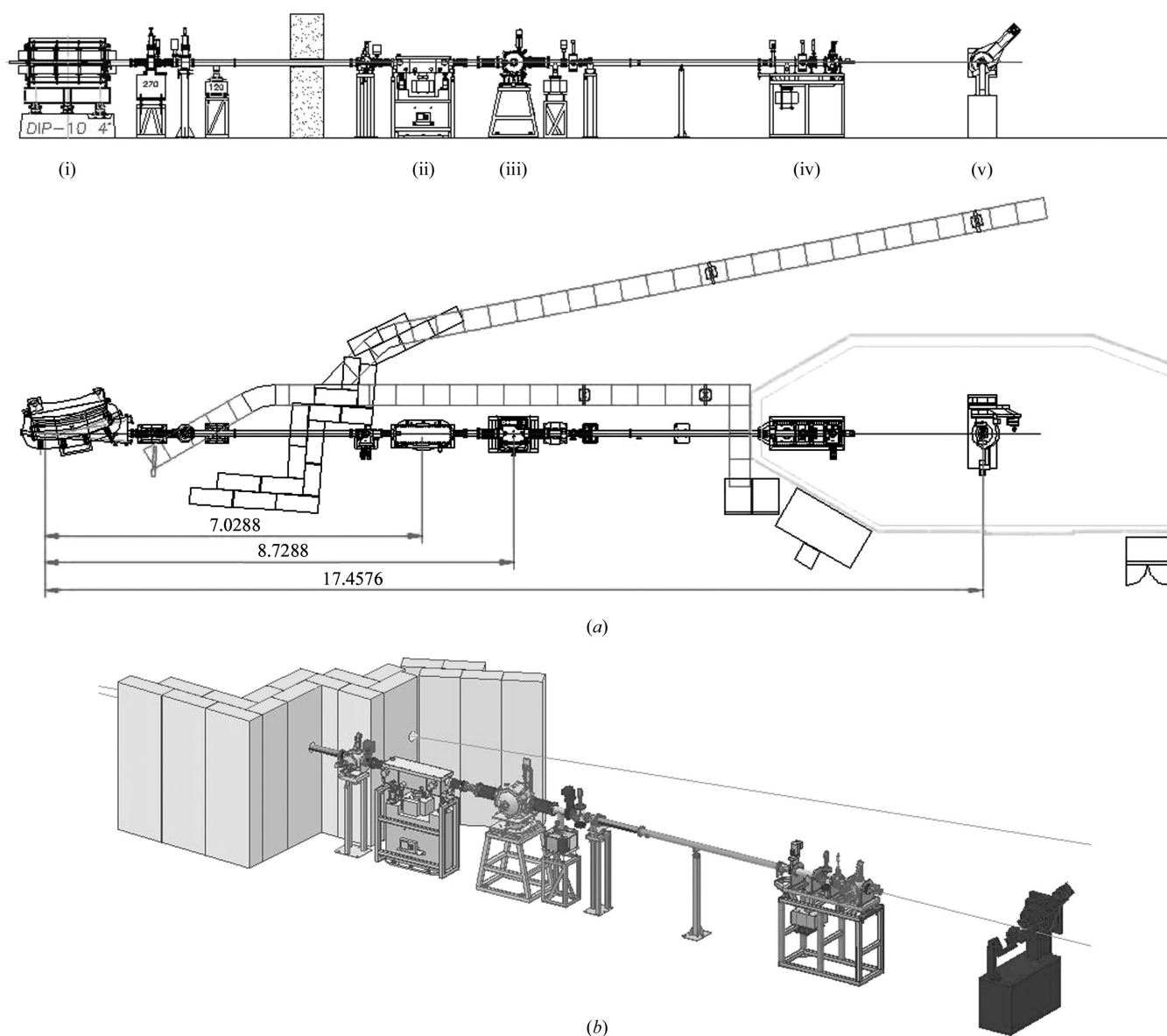


Figure 2

(a) Side and top views of the main components of the XRD2 beamline at LNLS: (i) bending-magnet source, (ii) X-ray mirror, (iii) double-crystal monochromator, (iv) end-station, (v) six-circle diffractometer. The total source-to-sample distance is 17.5 m and the sagittal-focusing monochromator is in a one-to-one configuration. (b) Schematic perspective view of the XRD2 beamline. The experimental hutch and other components are not shown for clarity.

3. Experimental end-station

The primary piece of equipment at the experimental end-station is a Huber six-circle diffractometer in the vertical-scattering geometry. If necessary, the diffractometer can be set to be used in the horizontal-scattering geometry by conveniently repositioning the main instrument on its motorized supporting stage. This equipment can be used in the four-circle mode or adjusted to perform experiments in three-circle geometry or grazing-incidence diffraction. High-resolution X-ray diffraction, small-molecule crystallography, as well as diffraction-enhanced imaging and phase-contrast radiography, are possible arrangements for this experimental end-station.

In order to perform non-resonant and resonant magnetic scattering, additional energy and polarization analysers are attached on the 2θ arm of the diffractometer (Fig. 3). Fast scintillator detectors, a highly purified Ge solid-state detector and Amptek pin-diodes are used for the scattering experiments. Ionization chambers and a CCD camera are used for alignment and position and intensity-monitoring purposes.

The sample environment consists of a closed-cycle helium cryostat with vibration damping and with temperature control within the 10–320 K range. A versatile Joule–Thomson cryostat is also available to control the sample temperature within the 90–700 K range. A magnetic field can be applied to the sample either using NdFeB permanent magnets at a fixed distance or by the use of electro-magnetic coils.

The diffractometer is operated using *SPEC* software (Certified Scientific Software, 1992) in a PC-based Linux environment. Recent upgrades of the beamline-control hardware allow the beamline monochromator to be controlled by *SPEC*, opening the way to performing resonant-scattering experiments with fixed- Q energy scans.

4. Magnetic scattering in NiO and Ho and orbital ordering in manganites

X-ray magnetic scattering was first performed on a NiO crystal at a conventional source laboratory (de Bergevin & Brunel, 1972). Improved measurements were performed later at second- (Hill *et al.*, 1997) and third-generation synchrotron sources (Fernandez *et al.*, 1998). As a test probe for this high-resolution scattering beamline, we

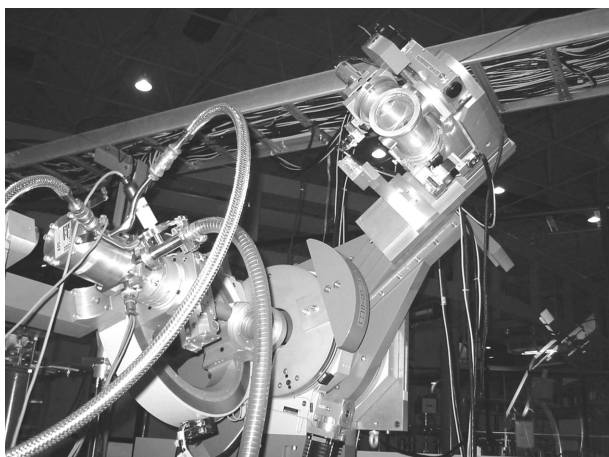


Figure 3 Six-circle Huber diffractometer with polarization analyser and displx cryostat used for resonant scattering of a Ho sample at the XRD2 beamline.

have reproduced non-resonant magnetic scattering from NiO. A NiO single crystal was cut ((111) orientation) and the surface was prepared following a known procedure for this material (Barbier *et al.*, 1999). The measurement was performed at 8200 eV, well below the Ni K edge. NiO orders in the type-II antiferromagnetic structure where ferromagnetic planes are stacked antiferromagnetically along the [111] axes with their magnetic moments aligned along one of the $[11\bar{2}]$ directions. A Fe layer was deposited on the NiO single crystal in order to study the magnetic coupling at the Fe/NiO interface. The interaction among spins in antiferromagnetic/ferromagnetic interfaces is known as exchange bias coupling. Although it was discovered in 1956 by Meiklejohn and Bean (Meiklejohn & Bean, 1956), many aspects of this problem remain open. Recently, results have been reported on the influence of the domain structure of the antiferromagnetic layer on the exchange coupling (Sampaio *et al.*, 2003). Thus, a careful azimuthal dependence study of the X-ray magnetic diffraction could provide information about the coupling mechanism involving antiferromagnetic domains and the exchange coupling. A typical rocking curve of the $(\frac{3}{2} \frac{3}{2} \frac{3}{2})$ magnetic reflection is presented in Fig. 4. This measurement was performed at room temperature, and was recorded using a scintillator detector with a single-channel analyser set narrowly to exclude the second-harmonic contamination already reduced by the Si(111) crystal monochromator. Additional scattering from the Fe layer contributes to the increased background noise around the magnetic peak. The temperature dependence of this magnetic reflection shows an expected intensity vanishing at around 523 K, demonstrating the magnetic nature of this reflection (Fig. 4, inset). The intensity count rate at the peak was of the order of 40 counts s^{-1} , comparable with results at second-generation sources (Hill *et al.*, 1997).

Resonant scattering is an important tool for exploring electronic properties of solids where interesting information can be obtained combining local probe techniques with long-range correlations. Resonant magnetic scattering was first observed in a single crystal of Ho, tuning the incident photon energy through the L_3 edge. A 50-fold increase in the integrated intensity was observed (Gibbs *et al.*, 1988). Resonant magnetic scattering in a Ho single-crystal sample oriented in the (100) orientation was performed at the XRD2 beamline. The expected resonant increase and polarization analysis has been

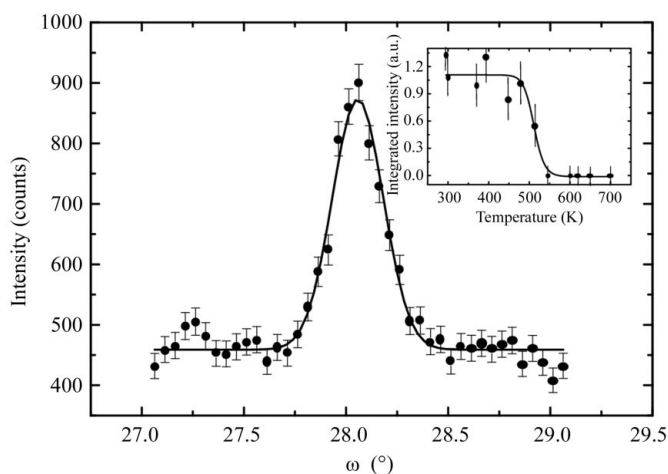


Figure 4 NiO magnetic-scattering rocking curve of the $(\frac{3}{2} \frac{3}{2} \frac{3}{2})$ reflection. $E = 8200$ eV, $T = 298$ K. The count rate is accumulated in 10 s. The crystal mosaicity is around 0.3° and the intensity ratio to the Bragg peak is as expected. The inset shows a temperature dependence of the integrated intensity with a decrease in intensity at around 530 K.

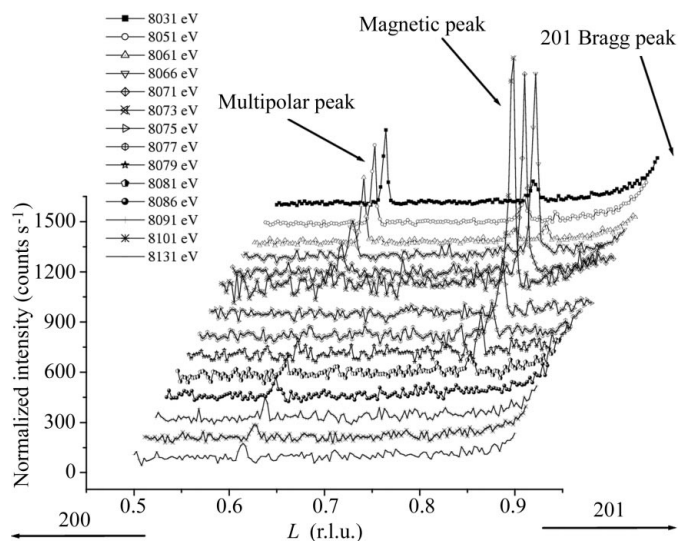


Figure 5 Resonant-scattering results for a Ho single-crystal plate with (100) orientation. The plot shows the evolution of the reciprocal space scans in the L direction as the energy of the incoming beam is changed across the L_3 edge of Ho at 8071 eV. The appearance of extra peaks at different positions is a signature of multipolar scattering of Ho.

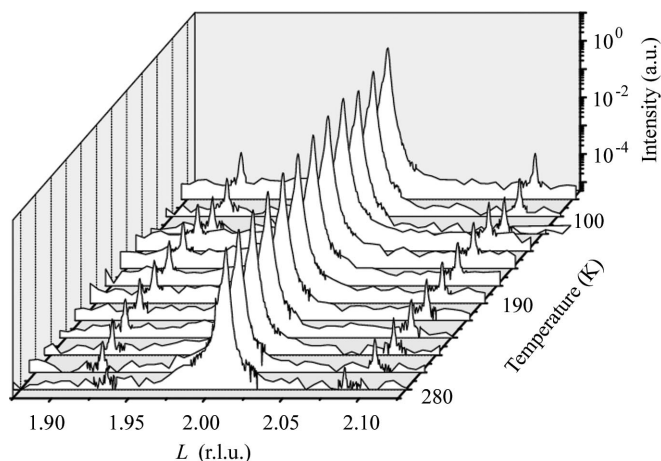


Figure 6 Temperature dependence of charge-density wave peaks of a Cr alloy single crystal. The evolution of the discommensuration with temperature variation allows direct measurement of the temperature dependence of the charge-density wave period.

reproduced in our data. Fig. 5 shows L scans of the magnetic peak $201-\tau$ for different incident energies from 8031 eV passing through the resonance at 8071 eV and reaching 8131 eV, well above the Ho L_3 edge. The presence of satellite peaks from multipolar scattering was favoured by the orientation of the crystal and is being published elsewhere (Yokaichiya & Giles, 2003).

As another example of magnetic materials studied at the XRD2 beamline, we report measurements of charge-density wave peaks of Cr and Cr alloys. Fig. 6 shows a temperature-dependence study of the modulation vector δ as a function of temperature measured in a Cr 0.18 at.% Re single crystal. Systematic studies of the integrated intensities of the charge-density wave peaks allow the independent measurement of the charge-density wave from the strain wave existing in the Cr alloys and dependent on the very small impurity quantity in this system (Yokaichiya, 1998). Further experiments at a

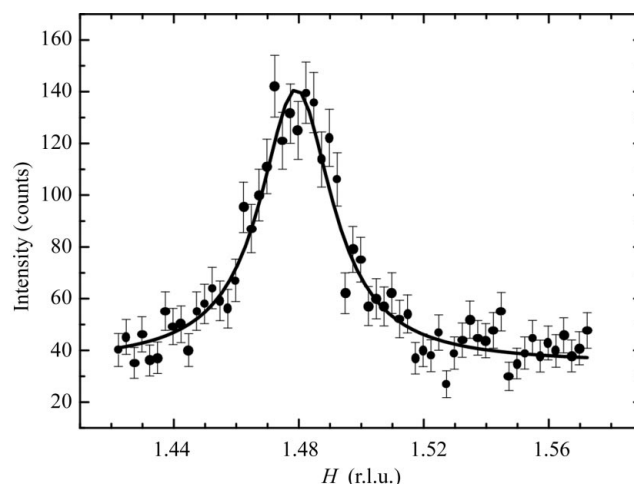


Figure 7 Orbital-ordering peak of a $\text{Pr}_{0.6}\text{Ca}_{0.4}\text{MnO}_3$ thin film on LaAlO_3 substrate. $E = 6539 \text{ eV}$, $T = 10 \text{ K}$, $\sigma-\sigma$ graphite analyzer. The thickness of the film is about 1800 \AA and this configuration introduces a compressive strain on the film. The H scan was measured at the $(\frac{3}{2} 2 0)$ reciprocal point as a function of the incoming energy and its maximum coincides with the K edge of Mn.

third-generation source allowed the determination of zero orbital magnetization of the spin-density wave with non-resonant magnetic scattering as well as a resonant signal at the K edge of Cr arising primarily from dipole transitions from the core $1s$ level to the $4p$ states (Mannix *et al.*, 2001).

Fig. 7 exhibits an orbital-ordering observation of a $\text{Pr}_{0.6}\text{Ca}_{0.4}\text{MnO}_3$ thin-film sample deposited on a LaAlO_3 substrate under a compressive strain condition. The $(\frac{3}{2} 2 0)$ reflection was measured at the K edge of Mn (6539 eV) and a graphite polarization analyser was able to distinguish the $\sigma-\sigma$ channel. This peak vanishes at energies away from the resonant condition and is compatible with similar measurements performed on bulk samples. Extensive studies on manganites thin films are underway and will be reported elsewhere (Nelson *et al.*, 2003), and systematic studies of orbital ordering in transition-metal oxides is underway at our beamline (Granado & Giles, 2003).

5. Summary and conclusions

XRD2 is a high-resolution X-ray diffraction beamline initially commissioned for magnetic-scattering techniques. The beamline optics and experimental end-station are well suited for resonant and non-resonant magnetic-scattering experiments as demonstrated by measurements on single crystals of NiO and Ho. Orbital-ordering studies are a potential technique to be exploited at this beamline owing to the possibility of performing resonant-scattering experiments with polarization analysis of the scattered beam. The beamline is now open for external users in the usual peer-review process of the LNLS. The potential use of the beamline for self-assembled nanocrystals and nanostructures has been demonstrated (Magalhães-Paniago *et al.*, 2002) and is presently a current technique at XRD2. Another potential application related to high-resolution phase-contrast X-ray imaging will be presented in a forthcoming publication (Giles *et al.*, 2003).

We would like to acknowledge the LNLS technical staff that greatly contributed to the installation and commissioning of the XRD2 beamline. This work was partially supported by the Conselho

Nacional de Desenvolvimento Científico e Tecnológico (CNPq), Fundação de Amparo à Pesquisa do Estado de São Paulo (FAPESP) and Programa de Apoio a Núcleos de Excelência (PRONEX). The X-ray magnetic-scattering end-station of the XRD2 beamline is supported by a grant from FAPESP (contract 96/05586-6) which is gratefully acknowledged. FY acknowledges a PhD grant from CNPq.

References

- Barbier, A., Renaud, G., Mocuta, C. & Stierle, A. (1999). *Surf. Sci.* **435**, 761–764.
- Bergevin, F. de & Brunel, M. (1972). *Phys. Lett. A*, **39**, 141.
- Certified Scientific Software (1992). *SPEC*. Certified Scientific Software, PO Box 802168, Chicago, IL 60680, USA.
- Correa, M. C., Tolentino, H., Craievich, A. F. & Cusati, C. (1992). *Rev. Sci. Instrum.* **63**, 896–898.
- Fernandez, V., Vettier, C., de Bergevin, F., Giles, C. & Neubeck, W. (1998). *Phys. Rev. B*, **57**, 7870–7876.
- Gibbs, D., Harshman, D. R., Isaacs, E., McWhan, D. B., Mills, D. & Vettier, C. (1988). *Phys. Rev. Lett.* **61**, 1241–1244.
- Giles, C., Honnicke, M. C., Lopes, R. T., Rocha, H., Gonçalves, O. D., Mazzaro, I. & Cusatis, C. (2003). *J. Synchrotron Rad.* **10**, 421–423.
- Granado, E. & Giles, C. (2003). LNLS Research Project XRD2-1565/02. LNLS, Campinas, Brazil.
- Hill, J. P., Kao, C. C. & McMorrow, D. F. (1997). *Phys. Rev. B*, **55**, R8662–R8665.
- Magalhães-Paniago, R., Medeiros-Ribeiro, G., Malachias, A., Kycia, S., Kamins, T. I. & Williams, R. S. (2002). *Phys. Rev. B*, **66**, 245312-1–245312-6.
- Mannix, D., de Camargo, P. C., Giles, C., de Oliveira, A. J. A., Yokaichiya, F. & Vettier, C. (2001). *Eur. Phys. J. B*, **20**, 19–25.
- Meiklejohn, W. P. & Bean, C. P. (1956). *Phys. Rev.* **102**, 1413.
- Nelson, C. S., Hill, J. P., Gibbs, D., Rajeswari, M., Biswas, A., Sharma, A., Venkatesan, T., Millis, A. J., Yokaichiya, F., Giles, C., Casa, D., Venkataraman, C. T. & Gog, T. (2003). In preparation.
- Neuenschwander, R. T. (2002). Unpublished.
- Sampaio, L. C., Mougín, A., Ferré, J., Georges, P. & Brun, A. (2003). *Europhys. Lett.* **63**, 819.
- Sparks, C. J., Ice, G. E., Wong, J. & Batterman, B. W. (1982). *Nucl. Instrum. Methods*, **195**, 73–78.
- Yokaichiya, F. (1998). Master's Degree thesis, Universidade Estadual de Campinas, Brazil.
- Yokaichiya, F. & Giles, C. (2003). In preparation.